Supporting information for:

Intermolecular Vibration Modes Speed Up Singlet Fission in Perylenediimide Crystals

Nicolas Renaud* and F. Grozema*

Opto-Electronic Materials Section, Department of Chemical Engineering, Delft University of Technology, Julianalaan 136, 2629BL, Delft, The Netherlands

E-mail: n.r.renaud@tudelft.nl; f.grozema.tudelft.nl

Contents

*To whom correspondence should be addressed

Derivation of the master equation

The derivation given below combines those given in Ref.[S1] chapter 3 and[S2] chapter 3. The reader can refer to these books for more details. At the difference with the derivation given in these references, two set of phonons are considered here which slightly complicates the derivation. When accounting for both intramolecular (Holstein) and intermolecular (Peierls) phonon modes, the total Hilbert space contains three distinct subspace: the excitons, the intramolecular phonon and the intermolecular phonon modes. Hence the total density matrix in the Born approximation reads:

$$\rho(t) = \rho_{\text{ex}}(t) \otimes \rho_{B_H} \otimes \rho_{B_P} \tag{1}$$

$\rho_{\text{ex}}(t)$ is the excitonic reduced density matrix (RDM) and $\rho_{B_H}(\rho_{B_P})$ the Holstein(Peierls) RDM. The derivation of the master equation (3) starts with the second order time-convolutionless equation of motion for the reduced density matrix in the interaction picture

$$\frac{d}{dt}\rho_{\text{ex}}(t) = -\int_0^t d\tau \,\text{Tr}_B\Big(\big[\mathscr{H}_{\text{ex-ph}}(t),[\mathscr{H}_{\text{ex-ph}}(t-\tau),\rho(t)]\big]\Big) \tag{2}$$

where the trace is performed over both the Holstein and the Peierls subspace, i.e. $\text{Tr}_B(\quad) = \text{Tr}_{B_H}(\text{Tr}_{B_P}(\quad))$ The double commutator comes from the perturbative treatment of the ex-ph interactions here taken at the second order only. Expending these commutator this equation can be rewritten as:

$$\begin{aligned}\frac{d}{dt}\rho_{\text{ex}}(t) &= \int_0^t d\tau \,\text{Tr}_B\Big(\mathscr{H}_{\text{ex-ph}}(t-\tau)\rho(t)\mathscr{H}_{\text{ex-ph}}(t) - \mathscr{H}_{\text{ex-ph}}(t)\mathscr{H}_{\text{ex-ph}}(t-\tau)\rho(t)\Big) \\ &+ \text{h.c.}\end{aligned} \tag{3}$$

The interaction Hamiltonian $\mathscr{H}_{\text{ex-ph}}$ encompass here both the Holstein and the Peierls interactions. We decompose here this interaction Hamiltonian as:

$$\mathscr{H}_{\text{ex-ph}} = \sum_m A_m^H \otimes B_m^H \otimes \mathbb{I} + \sum_m A_m^P \otimes \mathbb{I} \otimes B_m^P \tag{4}$$

where A_m^X (X=H,P) is an operator on the excitonic space and B_m^X an operator of the intramolecular (X=H) or intermolecular (X=P) subspace. To facilitate the description of $\mathscr{H}_{\text{ex-ph}}$ in the interaction picture we introduce the eigenoperators of the excitonic space. To do so let us denote the eigenvalues of $\mathscr{H}_{\text{ex}}$ by E_α, and the projection onto the subspace belonging to the eigenvalue E_α by $\Pi(E_\alpha) = |\Psi_\alpha\rangle\langle\Psi_\alpha|$. We can then define the eigenoperators as:

$$A_m^X(\omega) = \sum_{E_\alpha - E_\beta = \omega} \Pi(E_\alpha) A_m^X \Pi(E_\beta) \tag{5}$$

Since $A_m^X = \sum_\omega A_m^X(\omega)$ we can recast the interaction Hamiltonian as:

$$\mathscr{H}_{\text{ex-ph}} = \sum_{m,\omega} A_m^H(\omega) \otimes B_m^H \otimes \mathbb{I} + \sum_{m,\omega} A_m^P(\omega) \otimes \mathbb{I} \otimes B_m^P \tag{6}$$

Since the eigenoperators respect $[\mathscr{H}_{\text{ex}}, A_m(\omega)] = -i\omega A_m(\omega)$ we have $e^{i.\mathscr{H}_{\text{ex}}t} A_m(\omega) e^{-i.\mathscr{H}_{\text{ex}}t} = e^{-i\omega t} A_m(\omega)$. Hence the ex-ph interaction Hamiltonian in the interaction picture reads:

$$\mathscr{H}_{\text{ex-ph}}(t) = \sum_{m,\omega} e^{-i\omega t} A_m^H(\omega) \otimes B_m^H(t) \otimes \mathbb{I} + \sum_{m,\omega} e^{-i\omega t} A_m^P(\omega) \otimes \mathbb{I} \otimes B_m^P(t) \tag{7}$$

with $B_m^X(t) = e^{i.\mathscr{H}_{\text{ex}}t} B_m^X e^{-i.\mathscr{H}_{\text{ex}}t}$. This Hamiltonian can also be written as:

$$\mathscr{H}_{\text{ex-ph}}(t) = \sum_{m,\omega} e^{+i\omega t} A_m^{H\dagger}(\omega) \otimes B_m^{H\dagger}(t) \otimes \mathbb{I} + \sum_{m,\omega} e^{+i\omega t} A_m^{P\dagger}(\omega) \otimes \mathbb{I} \otimes B_m^{P\dagger}(t) \tag{8}$$

Introducing the density matrix (1) in eq. (3) and using the definitions (7) and (8), one obtains:

$$\begin{aligned} \frac{d}{dt}\rho_{\text{ex}}(t) &= \sum_{X=H,P} \sum_{m,m'} \sum_{\omega,\omega'} \Gamma_{mm'}^X(\omega,t) \Big(A_m^X(\omega) \rho_{\text{ex}}(t) \big(A_{m'}^X(\omega')\big)^\dagger - \big(A_m'^X(\omega')\big)^\dagger A_m^X(\omega) \rho_{\text{ex}}(t) \Big) e^{i(\omega-\omega')t} \\ &+ \text{h.c} \end{aligned} \tag{9}$$

where we have introduced the one-sided Fourier transform:

$$\Gamma^X_{mm'}(\omega,t) = \int_0^t d\tau\, e^{i\omega\tau} \mathrm{Tr}_{B_X}\left(\left(B^X_m(t)\right)^\dagger B^X_{m'}(t-\tau)\rho_{B_X}\right) \tag{10}$$

If ρ_{B_X} is a stationary state of the bath, then the bath correlation functions defined by $\langle \left(B^X_m(t_1)\right)^\dagger B^X_{m'}(t_2)\rangle \equiv \mathrm{Tr}_{B_X}\left(\left(B^X_m(t_1)\right)^\dagger B^X_{m'}(t_2)\rho_{B_X}\right)$ are homogeneous and therefore:

$$C^X_{mm'}(\tau) = \langle \left(B^X_m(t)\right)^\dagger B^X_{m'}(t-\tau)\rangle = \langle \left(B^X_m(\tau)\right)^\dagger B^X_{m'}(0)\rangle \tag{11}$$

Note that in the derivation of eq. (9) one encounters crossed terms such as:

$$\mathrm{Tr}_B\Big(A^H_m(\omega)\rho_{ex}(t)A^{P\dagger}_{m'}(\omega') \otimes B^H_m(t-\tau)\rho_{B_H} \otimes \rho_{B_P} B^{P\dagger}_{m'}(t)\Big) \tag{12}$$

where the Holstein and Peierls operators are mixed. These crossed terms are however null since we have supposed $\mathrm{Tr}_B[\mathscr{H}_{\text{ex-ph}}(t),\rho(0)] = 0$ to derive eq. (3) and therefore

$$\langle B^X_m(t)\rangle \equiv \mathrm{Tr}_{B_X}\left(B^X_m(t)\rho_{B_X}\right) = 0 \tag{13}$$

The secular approximation is then invoked to eliminate the terms $\omega \neq \omega'$ in eq. (9). We now define the bath operators as:

$$B^X_m = \Big[\sum_i \lambda_i^X \omega_i^X (b_i^X + b_i^{X\dagger})\Big]_m \tag{14}$$

where ω_i^X is the vibration frequency and λ_i^X the ex-ph interaction strength of the mode. Hence we assume that each operator A^X_m interact separately with its own set of phonon. While this assumption is not rigorously exact, it allows to write the bath correlation function as

$$C^X_{mm'}(t) = \delta_{mm'} C^X_{mm'}(t) \tag{15}$$

and therefore $\Gamma_{mm'}(\omega,t) \propto \delta_{mm'}$. We also suppose that all the Holstein operators interact with an

identical set of phonons. We make the same assumption for the Peierls operators. Hence the index m of $\Gamma_m^X(\omega,t)$ can be dropped. Therefore the master equation can be finally written as

$$\frac{d}{dt}\rho_{\rm ex}(t) = \sum_{X=H,P}\sum_{m,\omega}\Gamma_X(\omega,t)\Big(A_m^X(\omega)\rho_{\rm ex}(t)\big(A_m^X(\omega)\big)^\dagger - \frac{1}{2}\{\big(A_m^X(\omega)\big)^\dagger A_m^X(\omega),\rho_{\rm ex}(t)\}\Big) \quad (16)$$

It is convenient to decompose the Fourier transform of the bath correlation function as

$$\Gamma_X(\omega,t) = \frac{1}{2}\gamma^X(\omega,t) + i\eta^X(\omega,t) \quad (17)$$

with

$$\begin{aligned}\gamma_X(\omega,t) &= 2{\rm Re}\Big(\int_0^t ds e^{i\omega s}C_m^X(s)\Big) &(18)\\ \eta_X(\omega,t) &= {\rm Im}\Big(\int_0^t ds e^{i\omega s}C_m^X(s)\Big) &(19)\end{aligned}$$

After introducing this decomposition in eq. (16) and transforming back in the Schrodinger picture one obtain the equation

$$\begin{aligned}\frac{d}{dt}\rho_{\rm ex}(t) &= -i\big[\mathscr{H}_{\rm ex}+\mathscr{H}_{LS}(t),\rho_{\rm ex}(t)\big] + \sum_{X=H,P}\sum_{m,\omega}\gamma_X(\omega,t)\\ &\times \Big(A_m^X(\omega)\rho_{\rm ex}(t)A_m^X(\omega)^\dagger - \frac{1}{2}\{A_m^X(\omega)^\dagger A_m^X(\omega),\rho_{\rm ex}(t)\}\Big) \quad (20)\end{aligned}$$

The Hamiltonian $\mathscr{H}_{LS}(t) = \sum_X\sum_{m\omega}\eta_X(\omega,t)A_m^X(\omega)^\dagger A_m^X(\omega)$ leads to a Lamb-type renormalization of the coherent oscillation frequencies. This Hamiltonian is neglected in the following as they do not bring new features to the excitonic dynamics and are computationally expensive. The key elements of the non-Markovian dynamics is time dependence of the rates $\gamma^X(\omega,t)$. These rates are given by the integration of the time-dependent bath correlator $C^X(t)$. The anti-symmetric Fourier

transform of the bath correlator is given by:

$$C^X(t) = \int_0^\infty \frac{d\omega}{2\pi}\Big(e^{-i\omega t}[1+n(\omega)]C^{X^-}(\omega) + e^{i\omega t}n(\omega)C^{X^-}(\omega)\Big) \tag{21}$$

where $n(\omega)$ is the Bose-Einstein distribution and where the Fourier transform of the antisymmetric part of the correlation function given by:

$$C^{X^-}(\omega) = 2\pi\hbar^2\omega^2\big(\mathscr{J}_X(\omega) - \mathscr{J}_X(-\omega)\big) \tag{22}$$

Using this expression one obtain the expression of the time-dependent relaxation rate at finite temperature:

$$\begin{aligned}
\gamma_X(\omega,t) &= 2\mathrm{Re}\Big(\int_0^t ds e^{i\omega s}C^X(s)\Big) &(23)\\
&= 2\int_0^\infty d\nu\, \mathscr{J}_X(\nu)\Big[[1+n(\nu)]\frac{\sin(\omega-\nu)t}{\omega-\nu} + n(\nu)\frac{\sin(\omega+\nu)t}{\omega+\nu}\Big] &(24)
\end{aligned}$$

If required one can also obtain the expression of the time-dependent Lamb shift given by :

$$\begin{aligned}
\eta_X(\omega,t) &= \mathrm{Im}\Big(\int_0^t ds e^{i\omega s}C^X(s)\Big) &(25)\\
&= \int_0^\infty d\nu\, \mathscr{J}_X(\nu)\big[[1+n(\nu)]\frac{\cos(\omega-\nu)t}{\omega-\nu} + n(\nu)\frac{\cos(\omega+\nu)t}{\omega+\nu}\big]
\end{aligned}$$

Non-Markovian quantum jumps

Method

A complete presentation of the NMQJ approach can be found in the original reference.[S3] A brief description of the method is reported here for completeness. The master equation 3 is precisely

in the form required to employ the NMQJ technique. To unravel the dynamics generated by this local in time non-Markovian equation is solved using an ensemble of N stochastic pure states. The dynamics of each ensemble members is determine by a deterministic evolution interrupted by stochastic quantum jumps operated by the operators $A_m(\omega)$. As demonstrated in,[S4] the average dynamics of this ensemble of state vectors is rigorously equivalent to the solution of eq. 3. At any give time the ensemble density matrix can be expressed as:

$$\rho(t) = \frac{N_0(t)}{N}|\Psi_0(t)\rangle\langle\Psi_0(t)| + \sum_{\alpha=1}^{M}\frac{N_\alpha(t)}{N}|\Psi_\alpha(t)\rangle\langle\Psi_\alpha(t)| \tag{26}$$

where $|\Psi_0(t)\rangle$ is the initial state of the dynamics expressed in the excitonic basis and hash a weight of $N_0(t)/N$ in the ensemble. The eigenstates of the system $|\Psi_\alpha\rangle$ have been introduced earlier and acquired a time dependent phase factor during the time evolution. These eigenstates have a weight of $N_\alpha(t)/N$ in the ensemble. At all time the number of states in the ensemble is conserved, i.e. $N_0(t) + \sum_\alpha N_\alpha(t) = N$. The dynamics consists in time steps δt where any propagated state vector can either evolves in a deterministic fashion or undergo a stochastic quantum jump. The stochastic jumps only affects the statistical weights.

If the rate $\gamma_X(\omega,t)$ is positive, the jump operators $A_m(\omega)$ can transfer ensemble members from any propagated state $|\Psi_\alpha\rangle$ to the jump's target state $|\Psi_\beta\rangle$. The probability of such referred to as Markovian jump, is proportional to the decay rate, $\gamma_X(\omega,t)$, the duration of the time step, δt and the occupation of the decay state:

$$P^X_{\alpha\to\beta}(t,\omega,m) = \gamma_X(\omega,t)\delta t\langle\Psi_\alpha(t)|A^X_m(\omega)^\dagger A^X_m(\omega)|\Psi_\alpha(t)\rangle \tag{27}$$

If during the time interval δt, n ensemble members jumps from $|\Psi_\alpha\rangle$ to $|\Psi_\beta\rangle$ then one has to readjust the statistical weight as: $N_\alpha(t+\delta t) = N_\alpha(t) - n$ and $N_\beta(t+\delta t) = N_\beta(t) + n$. This procedure was already employed in the Markovian MCWF. The novelty of the NMQJ compared to the MCWF is the possibility for the relaxation rate to become negative. If the rate $\gamma_X(\omega,t)$ is

negative, a so-called non Markovian jump occurs. During time intervals where the rate is negative, the direction of the jump is reversed. The jump operator "undo" a Markovian jump that occurred earlier. Therefore ensemble members that has previously been transferred from state $|\Psi_\alpha(t)\rangle$ into state $|\Psi_\beta(t)\rangle$ by a Markovian jump can be transferred back into $|\Psi_\alpha(t)\rangle$ by a non Markovian jump when the rate is negative. The probability of such a non Markovian jump is given by:

$$P^X_{\alpha\leftarrow\beta}(t,\omega,m) = \frac{N_\alpha(t)}{N_\beta(t)}|\gamma_X(\omega,t)|\delta t\langle\Psi_\alpha(t)|A^X_m(\omega)^\dagger A^X_m(\omega)|\Psi_\alpha(t)\rangle \tag{28}$$

Note that if there is no ensemble members in the target state, $N_\alpha(t) = 0$, then probability to perform a non-Markovian from any state $|\Psi_\beta(t)\rangle$ back to $|\Psi_\alpha(t)\rangle$ is null. If during the time interval δt, n ensemble members jumps back from $|\Psi_\beta\rangle$ to $|\Psi_\alpha\rangle$ then one has to readjust the statistical weight as: $N_\alpha(t+\delta t) = N_\alpha(t) + n$ and $N_\beta(t+\delta t) = N_\beta(t) - n$.

As mentioned above the stochastic jump procedure described above is superimposed to a deterministic evolution of the state vectors $|\Psi_\alpha(t)\rangle$. Following the MCWF approach the deterministic evolution is generated by a non-Hermitian effective Hamiltonian:

$$\mathscr{H}_{\text{eff}} = \tilde{\mathscr{H}}_{\text{ex}} - \frac{i}{2}\sum_{X,\omega}\sum_m \gamma_X(\omega,t)A_m(\omega)^\dagger A_m(\omega) \tag{29}$$

A crucial element is the second term in the right hand side that is constructed from the jump operators present in eq. 3. Depending on the sign of $\gamma_{nm}(\omega,t)$ a given jump operator can either increase or decrease the occupation probability of the corresponding decay state. For each time step the deterministic evolution of the the state $|\Psi_\alpha(t)\rangle$ is performed by expanding the evolution operator to first order in time. We used a time symmetric expansion that respect time reversal symmetry and that is more stable numerically. The deterministic evolution during the time interval δt of state $|\Psi_\alpha(t)\rangle$ then reads:

$$|\Psi_\alpha(t+\delta t)\rangle = \frac{1 - i\mathscr{H}_{\text{eff}}\frac{\delta t}{2}}{1 + i\mathscr{H}_{\text{eff}}\frac{\delta t}{2}}|\Psi_\alpha(t)\rangle \tag{30}$$

According to eq. 29, the Hamiltonian $\mathscr{H}_{\text{eff}}$ is not Hermitian and therefore the norm of the wave function is not conserved under this deterministic evolution. The resulting state vector is consequently renormalized following:

$$|\Psi_\alpha(t+\delta t)\rangle = \frac{|\Psi_\alpha(t+\delta t)\rangle}{||\,|\Psi_\alpha(t+\delta t)\rangle\,||} \tag{31}$$

As mentioned earlier, the numerical procedure presented above is performed in the eigenbasis set of the system to insure that the final energy of the system is in thermal equilibrium with its environment. The population of the local state are then given by a simple rotation of the density matrix.

As clearly explained in the original paper the master equation 3 does not ensure that the density matrix remains positive. However the NMQJ allows to easily detect when the positivity of the density matrix is about to be violated. This happens if a given rate $\gamma_X(\omega,t)$ is negative and if there is no ensemble members in the source of the non Markovian jump anymore. In that case the the quantum non Markovian jump tries to undo undo a Markovian jump that has never occurred.

Application to an excitonic dimer

To illustrate the relative effect of resonant and off resonant spectral densities on the NM dynamics of a given quantum system we study here the time-dependent evolution of a excitonic dimer. The excitonic Hamiltonian of this simple system is:

$$\mathscr{H}_{\text{ex}} = \varepsilon_b|b\rangle\langle b| + J_{ab}\big(|b\rangle\langle a| + |a\rangle\langle b|\big) \tag{32}$$

This system could represent a minimal model for SF with the diabatic state $|a\rangle$ representing a double triplet state and $|b\rangle$ the singlet excited state. The exctionic states of the dimer, i.e. its eigenstates, are defined by : $|1\rangle = \sin\theta|a\rangle + \cos\theta|b\rangle$ and $|1\rangle = \cos\theta|a\rangle - \sin\theta|b\rangle$ with $\tan 2\theta = 2J_{ab}/\varepsilon_2$. We consider here that the phonon modes are described by a superOhmic spectral density

of the form;

$$\mathscr{J}_X(\omega) = \frac{\lambda_X}{\hbar\Omega_X}\,\omega^3 \exp\Big(-\frac{\omega}{\Omega_X}\Big) \tag{33}$$

We have set in the following $\Omega_H = 150$ meV, $\lambda_H = 50meV$, $\Omega_P = 10$ meV and $\lambda_P = 1$ meV. The time dependent rates obtained for the Holstein and Peierls spectral density with and excitonic transition of 0.1 eV are represented in Fig. S1. The Holstein spectral density is almost resonant with the transition frequency. Consequently the time-dependent rates converge rapidly to their Markovian limit. On the contrary the Peierls spectral density is off-resonant. The time dependent relaxation rates present then long living oscillations.

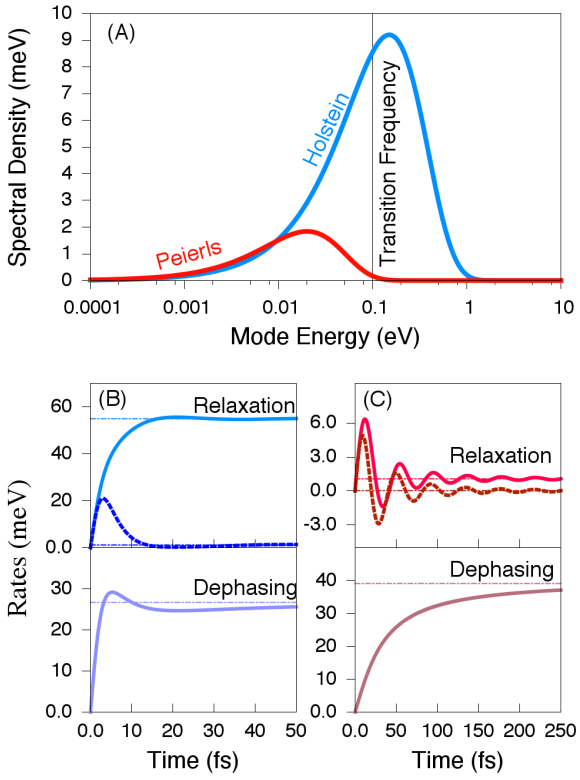

Figure S1: a) Spectral density corresponding to the Holstein and Peierls vibration modes. A given transition energy of 0.1 eV is represented.Time-dependent rate obtained for the Holstein (b) and Peierls (c) spectral density for a transition of 0.1 eV and T = 300 K. The corresponding Markovian rates are represented as dashed lines.

We first consider the case where only Holstein interactions are present in the system. Consequently each site interacts with its own individual set of phonons. The two Holstein diabatic operators are: $A_a^H = |a\rangle\langle a|$ and $A_b^H = |b\rangle\langle b|$. These two diabatic operators generate two excitonic relaxation operators : $A_b^H(\omega) = -A_a^H(\omega) = 1/2\sin 2\theta|1\rangle\langle 2|$ that correspond to energy relaxation from the excited to the ground state. Their complex conjugates: $A_b^H(-\omega) = -A_a^H(-\omega) = 1/2\sin 2\theta|2\rangle\langle 1|$ correspond to thermal reactivation from the ground to the excited excitonic state. Finally, the excitonic dephasing operators are given by: $A_a^H(0) = \sin^2\theta|1\rangle\langle 1| + \cos^2\theta|2\rangle\langle 2|$ and $A_b^H(0) = \cos^2\theta|1\rangle\langle 1| + \sin^2\theta|2\rangle\langle 2|$.

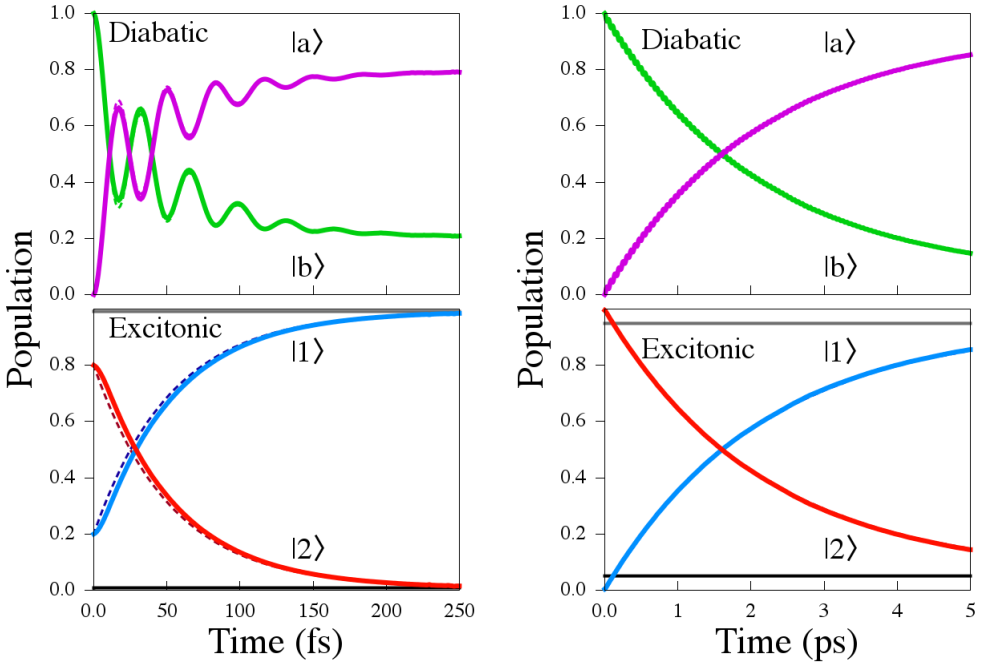

Figure S2: Dimer population evolution in the diabatic and excitonic base for a) $J_{ab} = 50$ meV and b) $J_{ab} = 5$ meV. The full line was obtained using time-dependent rates whereas the dashed lines correspond to the Markovian limit. The upper and lower dark lines shown superimposed to the excitonic populations shows the Boltzmann population of the excitonic states.

We show in Fig. S2 the population of the excitonic dimer presented above. Two cases are represented $J_{ab} = 50$ meV and $J_{ab} = 5$ meV. The site-energy ε_b was set to : $\varepsilon_b = 0.075$ eV. The

Holstein reorganization energy was set to $\lambda_H = 25$ meV and the cutoff frequency to $\Omega_H = 0.15$ eV. All these parameters are identical to the ones used in Ref.[S5] The population we obtain are almost identical to the ones obtained in Ref.[S5] using different simulation techniques. This confirm the validity of our implementation of the NMQJ approach.

Symmetry adapted basis

A symmetry adapted basis can be adopted to facilitate the description of SF.[S6] Taking the notation of Hamiltonian (2) of the main text, we define the new states:

$$|S_{\pm}\rangle = (\sqrt{2})^{-1}(|1\rangle \pm |2\rangle) \tag{34}$$

$$|CT_{\pm}\rangle = (\sqrt{2})^{-1}(|3\rangle \pm |4\rangle) \tag{35}$$

$$|TT\rangle = |5\rangle \tag{36}$$

Using these new states the Hamiltonian can be rewritten as:

$$\mathscr{H}_{\text{ex}} = \begin{array}{c} \begin{array}{ccccc} |S_+\rangle & |CT_+\rangle & |TT\rangle & |CT_-\rangle & |S_-\rangle \end{array} \\ \begin{pmatrix} E_{S_1S_0} & V_{LL}-V_{HH} & \sqrt{2}V_{2e} & 0 & 0 \\ V_{LL}-V_{HH} & E_{CT} & \frac{\sqrt{3}}{2}(V_{HL}+V_{LH}) & 0 & 0 \\ \sqrt{2}V_{2e} & \frac{\sqrt{3}}{2}(V_{HL}+V_{LH}) & E_{TT} & \frac{\sqrt{3}}{2}(V_{LH}-V_{HL}) & 0 \\ 0 & 0 & \frac{\sqrt{3}}{2}(V_{LH}-V_{HL}) & E_{CT} & V_{LL}+V_{HH} \\ 0 & 0 & 0 & V_{LL}+V_{HH} & E_{S_0S_1} \end{pmatrix} \end{array} \tag{37}$$

Note that $\langle S_-|\mathscr{H}_{\text{ex}}|TT\rangle = 0$. This indicate that only the state $|S_+\rangle$ is directly coupled to the double triplet state. Note also that if $V_{LL} = -V_{HH}$ and $V_{HL} = V_{LH}$, then the states $|CT_-\rangle$ and $|S_-\rangle$ are completely decoupled from the rest of the system. Then assuming that the initial state of the dynamics is $|S_+\rangle$, the SF dynamics can studied using a limited 3×3 matrix instead of the 5×5 to limit the computational cost. Finally if $V_{HL} = -V_{LH}$, the coupling $\langle CT_+|\mathscr{H}_{\text{ex}}|TT\rangle$ is null. Then the transfer from $|S_+\rangle$ to $|TT\rangle$ can only be mediated by the direct 2-electron coupling and not by the indirect pathway via the CT state.

Electronic Structure Calculation for PDI dimers

Energy of the excitonic states

The values of the singlet and triplet relaxed energies for the different PDI were obtained using standard TDDFT procedure.The geometry of the molecules were first relaxed in their singlet or triplet state using TDDFT gradients. This geometry optimization was done using different functionals (LDA/PBE/B3LYP) and a DZP basis set. The geometries obtained using PBE and B3LYP were almost identical and significantly different from the one obtained using LDA. We therefore used the geometry obtained at the B3LYP level of theory to compute the excitations.

These relaxed geometries were then used to compute the singlet and triplet excitation energies. A larger basis set (TZ2P) was used during these calculations and several functional were tested. The results obtained at the TZ2P/B3LYP level of theory for the 4 PDI derivatives represented in Fig. 1 as well as for the unsubstituted PDI are summarized on Table S1. Little variations among the different molecules were obtained for these different energies at the exception of the adiabatic triplet energies. This energy is unfortunately a important parameter of SF as it defines the energy of the final state:

$$E_{TT} = 2 \times E_T^{\text{adiabatic}} \tag{38}$$

To focus on the impact of the intermolecular mode only on SF we have kept kept the energies obtained for the unsubstituted PDI. Note however that an accurate determination of the adiabatic singlet and triplet energies is still difficult at the TDDFT level of theory. The values of these energies vary significantly with the functional used during the calculations. An adiabatic singlet and triplet energy of 2.22 eV and 0.70 eV was for example obtained for unsubstituted PDI at the TZ2P/PBE0 level of theory. These values would lead to an energy gap of 0.82 eV between the singlet excited states and the double triplet state. In this case the intermolecular mode would have a negligible impact on the SF dynamics. A great caution should therefore be exerted while

using these values to describe organic crystals, and these values should be taken as rough order of magnitude only.

Table S1: Excitation energies for different PDI obtained at the TZ2P/B3LYP level of theory

	vertical		adiabatic	
	E_S (eV)	E_T (eV)	E_S (eV)	E_T (eV)
PDI	2.35	1.23	2.17	0.95
1	2.41	1.32	2.16	0.86
2	2.42	1.32	2.16	1.00
3	2.40	1.32	2.15	0.87
4	2.42	1.34	2.13	1.10

Holstein ex-ph coupling

A linear expansion of the energy of the frontier molecular orbitals with respect to the intramolecular vibrational coordinate leads to a simple expression for the Holstein reorganization energy of each intramolecular vibration mode:[S7]

$$\lambda_j = \frac{1}{2M_j\omega_j^2}\left(\frac{d\varepsilon_m}{dQ_m(j)}\right)^2_{Q=0} \tag{39}$$

where ε_m is the energy of the state considered, M_j is the effective mass of the j-th intramolecular vibrational mode, ω_j its frequency and Q_j its vibrational coordinate. In order to o compute the values of λ_j, the geometry of each molecule was first relaxed using a DZP basis set and the PBE exchange-correlation functional. These fully relaxed geometries were then used to compute the vibrational modes of the molecules using the same basis set and functional. Subsequently, single point calculations using a TZ2P basis set and the B3LYP exchange-correlation functional were performed to numerically evaluate the derivatives of the HOMO, LUMO, singlet and triplet energies along each individual vibrational coordinate. The results of these calculations for an unsubstituted PDI are shown in Fig. S3. The results obtained for the 4 PDI derivatives were almost identical as the frontier molecular orbitals are localized on the core of the molecule, and therefore the substituents only marginally change the results.

All the molecules exhibit pronounced interactions between the charge and the vibrations modes centered around 0.15 eV. This value, which roughly corresponds to the C-C vibration mode, is therefore used to define the cutoff frequency of the bath spectral density, $\Omega = 0.15$ eV, in the following. The value of the reorganisation energy was here calculated following $\lambda = \sum_i \lambda_i$ and corresponding only the three most dominant contributions.

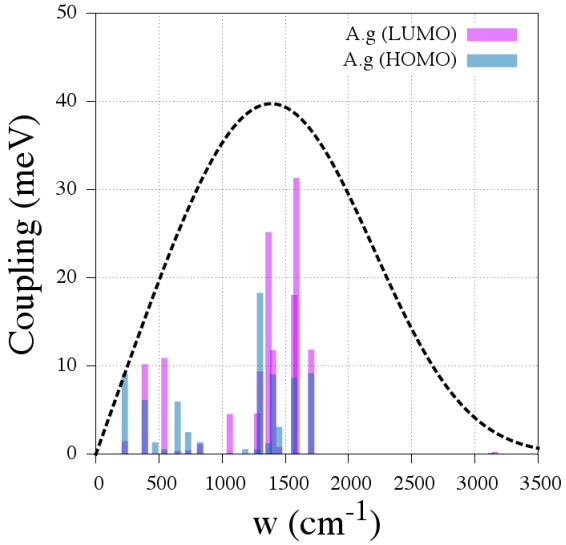

Figure S3: Holstein ex-ph interactions obtained for unsubstituted PDI

Peielrs ex-ph coupling

The Peierls reorganization energy was calculated using:[S7]

$$L_P(\omega_m(k)) = \frac{1}{2M\omega_m^2(k)} \left(\frac{dV_{2e}}{dQ(\omega_m(k))} \right)^2_{Q=0} \tag{40}$$

In eq. (40), $Q(\omega_m(k))$ is the vibration coordinate of the vibration mode on the m-th dispersion band with a wave vector k, M its effective mass and $\omega_m(k)$ its frequency. The intermolecular vibration modes were calculated by considering an 1D infinite stack of identical molecules similar to the one represented in Fig. S4. As seen on this figure a unit cell of two molecules (i.e. a dimer)

was considered. Due to this doubling of the unit cell the first Brillouin zone is folded leading to an accoustic and optical branch that are degenerated at the border of the zone. This doubling of the Brillouin zone is necessary to obtain the vibration coordinate of each molecule in the dimer for each vibration mode. These coordinate are required to compute the variation of the coupling along the modes.

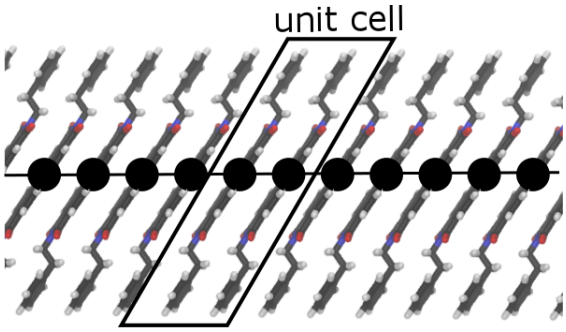

Figure S4: 1D infinite stack of molecules considered for the calculation of the intermolecular vibration modes of **1**.

The frequencies of the intermolecular vibration modes were evaluated in the harmonic approximation.

$$\omega_i(k) = 2\sqrt{K_i/M}\sin(k) \tag{41}$$

with $k = [-\frac{\pi}{2a}; \frac{\pi}{2a}]$ where a is the lattice parameter and $i = X,Y,Z$. To this end the variation of the binding energy of the dimer was calculated along the three axis mentioned above. These calculations were done at the DFT level of theory using a DZP basis set and the B3LYP functional. The variation of the binding energies obtained for molecule **1** are shown in Fig. S5. These variations were then fitted by an harmonic potential ($K(X-X_0)^2$) to obtain the corresponding values of K_i. The effective mass was taken as the mass of the dimer.

The variations of V_{2e} along the long axis (X), short axis (Y) or interplanar axis (Z) of the dimer, were calculated for all the molecules. The results obtained for molecule **2** are shown in Fig. S5. The derivative of the coupling was then numerically evaluated in all cases. The values of the K_i

and of the derivative of the binding energies along the cartesian axis are reported in table S2.

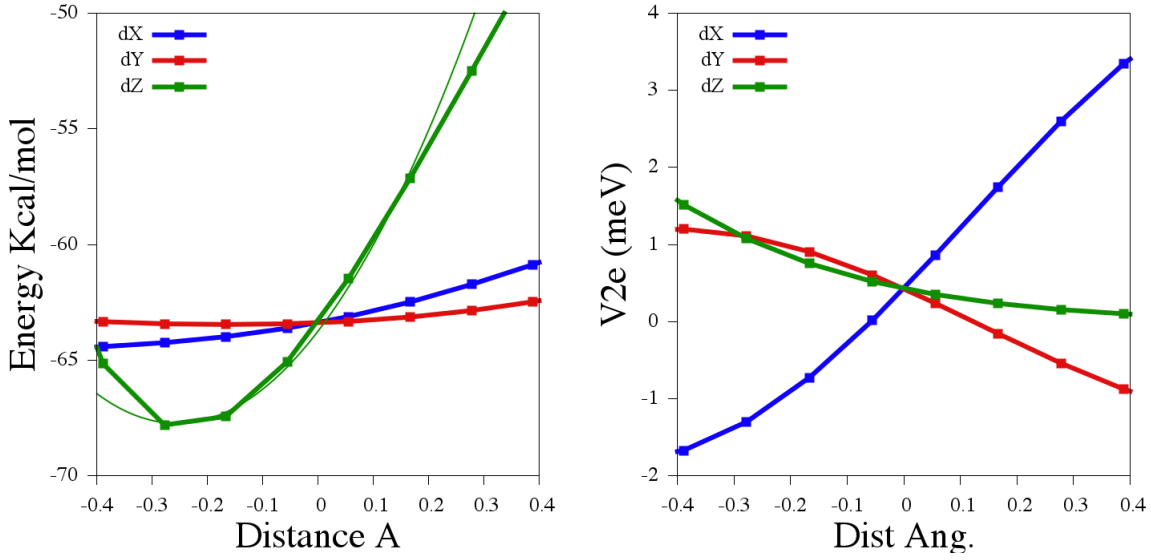

Figure S5: a) Variation of the binding energy of the dimer along the same axis. b) Variation of the 2 electron coupling along the X, Y and Z axis of the dimer obtained for **1**.

Table S2: Harmonic fit parameter of the binding energy (K_i) and of the derivative of of the 2-electron couplings (d_iV_{2e}) along the Cartesian axis

	kcal/mol			meV/Ang		
	K_X	K_Y	K_Z	d_xV_{2e}	d_yV_{2e}	d_zV_{2e}
1	4.61	3.13	51.12	7.77	2.75	3.68
2	4.23	2.98	48.94	16.22	15.48	14.54
3	11.97	35.53	13.11	0.31	0.48	0.01
4	9.87	14.12	47.71	11.45	11.23	10.27

The phonon dispersion obtained with this approach for molecule **1** is represented in Fig. S6. One can see on this figure that the phonon dispersion in the Z direction leads to much larger frequencies due to the larger values of K in that direction than in the X and Y direction. Using the value of the derivative of V_{2e} and the vibration coordinate of the modes one is then able to compute the the reorganization energy of the 2-electron coupling. This coupling is shown in Fig. S6. As seen in this figure the optical mode always provide the largest reorganization energy. Besides the values of L_P obtained along the Z direction are order of magnitude lower than those obtained in

the X and Y direction. This is principally due to the smaller derivative of V_{2e} in the Z direction as compared as the two other ones.

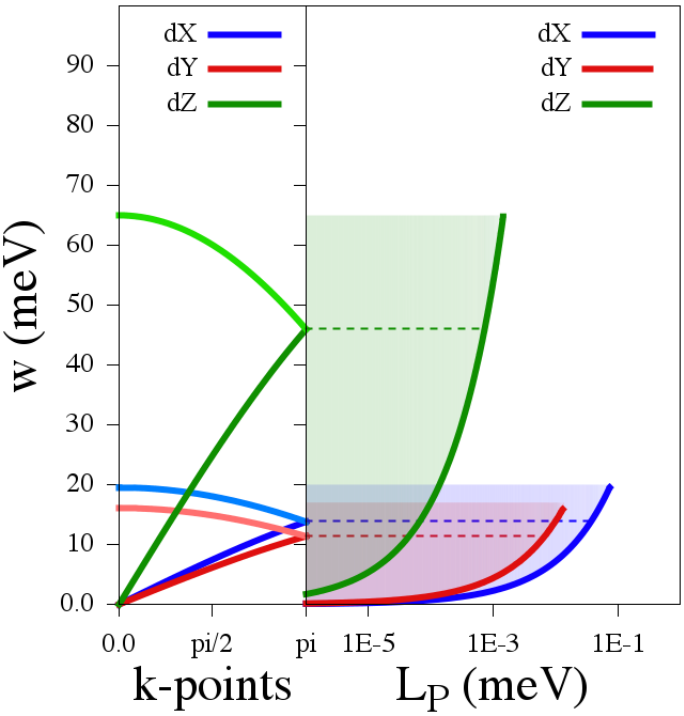

Figure S6: Left - Phonon dispersion calculated using the harmonic approximation presented above. Right - Corresponding ex-ph interaction strength

Fluctuation of the 1-electron couplings

Following the same approach outlined above for the calculations of the the Peierls coupling of the 2-electron coupling, we have computed the fluctuations of the 1-electron couplings and their associated Peierls reorganization energy. The results of these calculations for compounds **2** are reported in Fig. S7. As seen in this figure the spectral density associated with these fluctuations are much larger than those of V_{2e} reaching few meVs.

We have then included these fluctuations in the exciton dynamics. To do so we have changed the definition of the Peierls operators for the ex-ph interactions to: $A_1^P = A_2^{P^\dagger} = |1\rangle\langle 3|$, $A_3^P =$

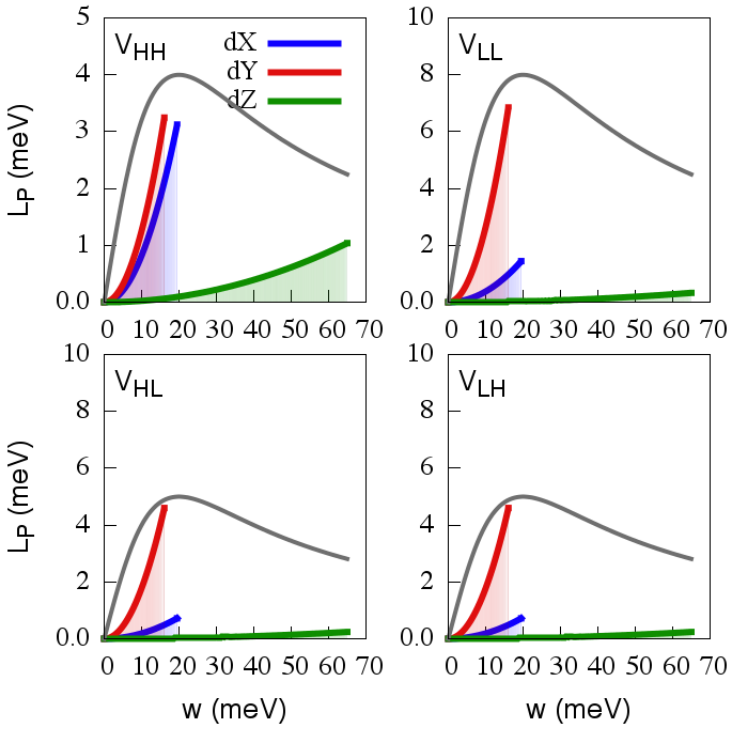

Figure S7: Reorganization energy induced by the fluctuations of the 1-electron couplings due to the intermolecular vibration modes for compound **2**.

$A_4^{P\dagger} = |1\rangle\langle 4|$, $A_5^P = A_6^{P\dagger} = |2\rangle\langle 3|$, $A_7^P = A_8^{P\dagger} = |2\rangle\langle 4|$, $A_9^P = A_{10}^{P\ \dagger} = |3\rangle\langle 5|$, , $A_{11}^P = A_{12}^{P\ \dagger} = |4\rangle\langle 5|$. We hence now neglect the fluctuations of the 2-electron coupling and exclusively account for those of the 1-electron couplings. The excitonic dynamics obtained with these new operators and the spectral density shown in Fig. S7 are reported in Fig. S8a. As seen in this figure the effect of the 1-electron coupling fluctuations is much less pronounced that those induced by the fluctuations of the 2-electron coupling. However if all the reorganization energy are set to 20 meV instead of the values shown in Fig. S7, the fluctuations of the 1-electron coupling have a similar impact than those of the 2-electron couplings (see Fig. S8b). The fluctuations of the 1-electron coupling could therefore have a significant impact of the SF dynamics in case where the their variations near the equilibrium geometry of the dimer are larger than those obtained here.

The little impact of the fluctuations of the 1-electron coupling can be easily understood looking at the relaxation rates. The Holstein interactions already introduce a fast relaxation between the

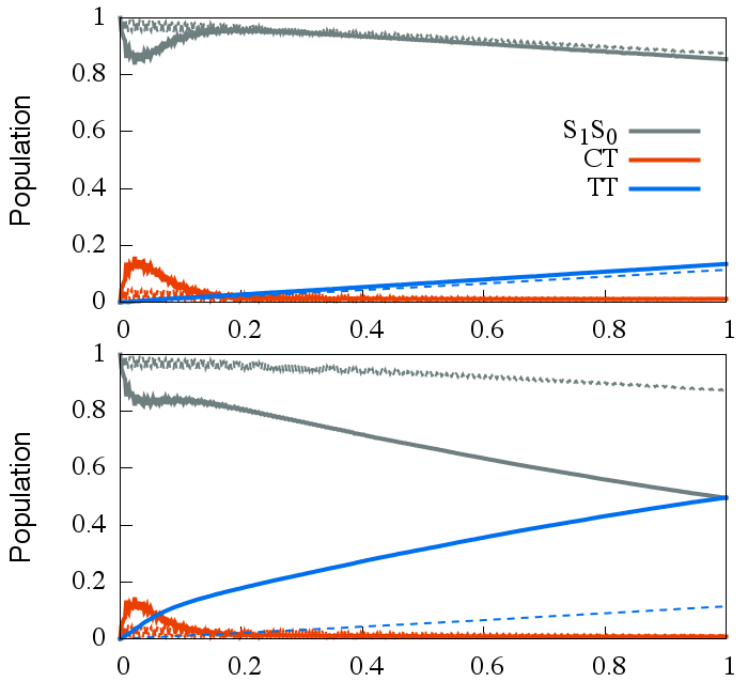

Figure S8: SF dynamics obtained in presence of fluctuations of the 1-electron couplings without (dashed line) and with (plain lines) Peierls coupling for top - reorganisation energy reported in Fig. S7, bottom - all reorganisation energy set to 20 meV.

singlet states and the CT states and also between the CT states and the double triplet states. This is due to the relatively strong values of the 1-electron coupling. Therefore adding the intermolecular modes only slightly increase these relaxation rates. As a consequence a strong values of the Peierls reorganization energy is required to observe a significant impact of the intermolecular vibration modes on the dynamics. On the contrary due to the weak value of V_{2e} the intramolecular vibration modes introduce a weak direct relaxation between S_1S_0 and TT. The introduction of the fluctuation of the 2-electron coupling therefore significantly improves this relaxation channel.

Impact of the initial state

For the PDI derivatives **1-3**, we have the condition $V_{HL} = -V_{LH}$. Therefore the excitonic Hamiltonian in the symmetry adapted basis reads:

$$\mathscr{H}_{\text{ex}} = \begin{array}{c} \begin{array}{ccccc} |S_+\rangle & |CT_+\rangle & |TT\rangle & |CT_-\rangle & |S_-\rangle \end{array} \\ \begin{pmatrix} E_{S_1S_0} & V_{LL}-V_{HH} & \sqrt{2}V_{2e} & 0 & 0 \\ V_{LL}-V_{HH} & E_{CT} & 0. & 0 & 0 \\ \sqrt{2}V_{2e} & 0 & E_{TT} & \sqrt{3}V_{LH} & 0 \\ 0 & 0 & \sqrt{3}V_{LH} & E_{CT} & V_{LL}+V_{HH} \\ 0 & 0 & 0 & V_{LL}+V_{HH} & E_{S_0S_1} \end{pmatrix} \end{array} \tag{42}$$

As seen on this Hamiltonian the state $|CT_+\rangle$ is not coupled to the double triplet state. Hence if the initial state of the dynamics is set to $|\Psi(0)\rangle = |S_+\rangle$ only the direct pathway supported by V_{2e} contribute to SF. On the contrary if the initial state is set to $|\Psi(0)\rangle = |S_-\rangle$ only the mediated by the CT state can lead to SF. Therefore the excitonic dynamics is very sensitive to the choice of the initial state and the Peierls interactions are then more or less important. To illustrate this we have plotted in Fig. S9 the SF dynamics obtained for **2** with different initial conditions: a) $|\Psi(0)\rangle = |S_+\rangle$, b) $|\Psi(0)\rangle = |S_-\rangle$, c) $|\Psi(0)\rangle = \sqrt{2}^{-1}(|S_+\rangle + |S_-\rangle)$ and d) $|\Psi(0)\rangle = \sqrt{2}^{-1}(|S_+\rangle - |S_-\rangle)$. In the case $|\Psi(0)\rangle = |S_+\rangle$, only the direct pathway support SF and therefore the Peierls couplings have a significant impact on the dynamics. On the contrary when $|\Psi(0)\rangle = |S_-\rangle$, the mediated pathways via the CT state is the main contribution to SF and then the Peierls have a minimal impact on the dynamics. In intermediate cases, both pathways play a role in SF and therefore the Peierls couplings plays also a role in the SF dynamics, albeit less pronounced than for $|\Psi(0)\rangle = |S_+\rangle$.

Note that in the case of **1**, $V_{LL}-V_{HH} = 270$ meV and $V_{LL}+V_{HH} = -20$ meV. Consequently a strong coupling exists between $|S_+\rangle$ and $|CT_+\rangle$. This large electronic coupling is responsible for the long lasting fast coherent oscillations observed in Fig. 1. On the contrary, the coupling between $|S_-\rangle$ and $|CT_-\rangle$ is relatively small (20 meV). Consequently, even when starting from $|S_-\rangle$ the SF dynamics remains slow.

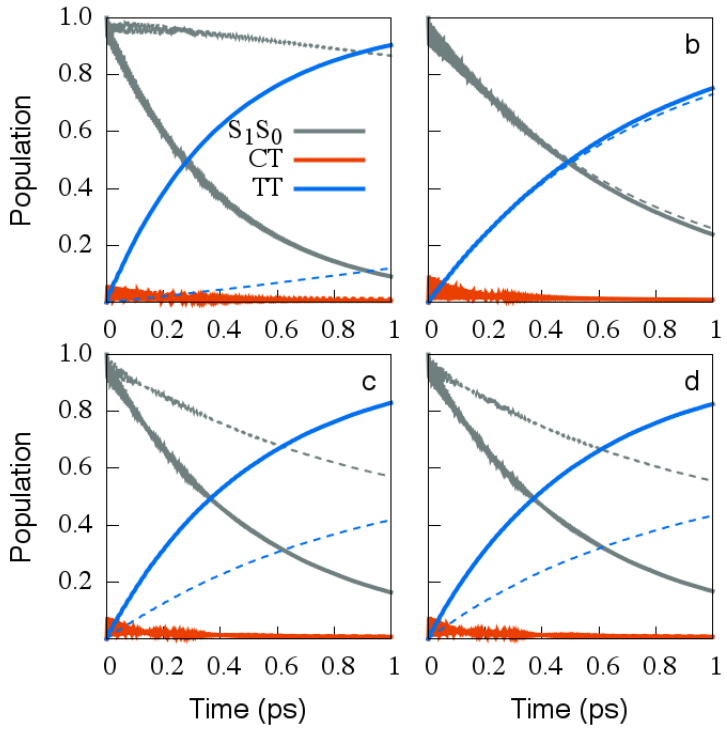

Figure S9: Population obtained for molecule **2** with different initial states: a) $|\Psi(0)\rangle = |S_+\rangle$, b) $|\Psi(0)\rangle = |S_-\rangle$, c) $|\Psi(0)\rangle = \sqrt{2}^{-1}(|S_+\rangle + |S_-\rangle)$ and d) $|\Psi(0)\rangle = \sqrt{2}^{-1}(|S_+\rangle - |S_-\rangle)$

Impact of the spectral density

As mentioned in the main text the choice of the spectral density can significantly influence the SF dynamics. Instead of the spectral density used in the main text one can choose different representation with different high-frequency cutoff. For example one can use the general form

$$\mathscr{J}(\omega) = \lambda \left(\frac{\omega}{\omega_c}\right)^{\mu} e^{(-\mu \frac{\omega}{\omega_c})} \tag{43}$$

Using this definition a subohmic density is obtained for $\mu < 1$, an Ohmic one for $\mu = 1$ and a superohmic for $\mu > 1$. The exponential high-frequency cutoff is here introduced to replace the Lorentzian one used in eq. (5). We have computed the SF dynamics of compounds **2** with different spectral densities for the Peierls coupling to understand its impact in the formation of the double triplet states. The spectral density of the Holstein interaction was still described as in the main text. The different spectral densities used here for the Peierls couplings are shown in Fig. S10a.

We used a subhomic density with $\mu = 1/2$ and a superohmic density with $\mu = 2$. The parameter λ_P needed to be adjusted in both cases to $\lambda_P = 0.65$ meV and $\lambda_P = 3.7$ meV respectively to obtain the fit shown in Fig. S10.

As seen in Fig. S10, the effect of the Peierls coupling is almost negligible for a superohmic spectral density (i.e. $\mu = 2$) while it remains important for a subohmic density (i.e. $\mu = 1/2$). This is due to the different high-frequency cutoff of these two spectral densities. For $\mu = 1/2$, $\mathscr{J}(\omega)$ remains quite large at $\omega = 0.27$ eV (i.e. the energy difference between $E_{S_1S_0}$ and E_{TT}). Hence the markovian relaxation rate induced by the Peierls coupling is not-negligble and the SF dynamics is improved by the intermolecular vibration modes. On the contrary for $\mu = 2$, $\mathscr{J}(\omega = 0.27\,eV) \simeq 0$ and the effect of the Peierls coupling is then negligible. The high frequency cutoff of the spectral density has therefore a significant influence on the dynamics.

Note however that in the case of a narrow spectral density such as the one obtained with $\mu = 2$, an important effect of the Peierls coupling can be retrieved if the difference between $E_{S_1S_0}$ and E_{TT} is reduced. Such calculation is shown in Fig. S10 where a value of $E_{S_1S_0} - E_{TT} = 100$ meV has been used. Note that in that case the SF dynamics obtained in absence of Peierls coupling is also slightly faster due to the smaller energy difference $E_{S_1S_0} - E_{TT}$ that enhance the incoherent transfer mediated by the Holstein interactions.

References

(S1) p. Breuer, H.; Petruccione, F. *The theory of Open Quantum Systems*; Oxford University Press, 2002.

(S2) May, V.; Kuhn, O. *Charge and Energy Transfer Dynamics in Molecular Systems*; Wiley-VCH, 2000.

(S3) Piilo, J.; Maniscalco, S.; Härkönen, K.; Suominen, K.-A. *Phys. Rev. Lett.* **2008**, *100*, 180402.

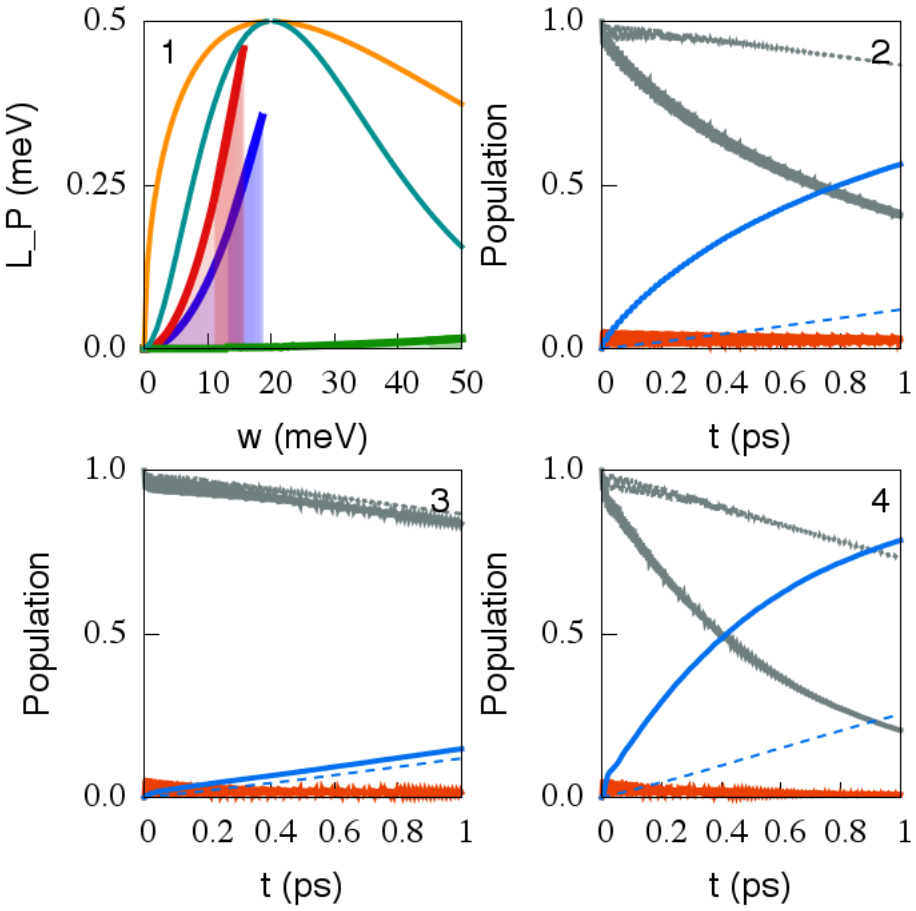

Figure S10: 1- Superohmic (blue) and subohmic (orange) fit to the spectral densities of the intermolecular vibration modes. 2 - SF dynamics obtained for **2** and a subohmic spectral density, 3 - SF dynamics obtained for **2** and a superohmic spectral density, 4 - SF dynamics obtained for **2** and a superohmic spectral density and $E_{S_1S_0} - E_{TT} = 100$ meV.

(S4) Piilo, J.; Härkönen, K.; Maniscalco, S.; Suominen, K.-A. *Phys. Rev. A* **2009**, *79*, 062112.

(S5) Berkelbach, T. C.; Hybertsen, M. S.; Reichman, D. R. *The Journal of Chemical Physics* **2013**, *138*, 114102.

(S6) Wang, L.; Olivier, Y.; Prezhdo, O. V.; Beljonne, D. *The Journal of Physical Chemistry Letters* **2014**, *5*, 3345–3353.

(S7) Coropceanu, V.; Cornil, J.; da Silva Filho, D. A.; Olivier, Y.; Silbey, R.; Brédas, J.-L. *Chem. Rev.* **2007**, *107*, 926–952.